BULLETIN OF THE POLISH ACADEMY OF SCIENCES
TECHNICAL SCIENCES
Vol. 55, No. 2, 2007

Discrete-continuum transition at interfaces of nanocomposites

R. PYRZ[1*] and B. BOCHENEK[2]

[1]Department of Mechanical Engineering, Aalborg University, 101Pontoppidanstrade St., 9220 Aalborg East, Denmark
[2]Institute of Applied Mechanics, Cracow University of Technology, 37 Jana Pawla II St., 31-864 Cracow, Poland

Abstract. A number of micromechanical investigations have been performed to predict behaviour of composite interfaces, showing that the detailed behaviour of the material at these interfaces frequently dominates the behaviour of the composite as a whole. The interfacial interaction is an extremely complex process due to continuous evolution of interfacial zones during deformation and this is particularly true for carbon nanotubes since the interfacial interaction is confined to the discrete molecular level. The atomic strain concept based upon Voronoi tessellation allows analyzing the molecular structure atom by atom, which may give a unique insight into deformation phenomena operative at molecular level such as interface behaviour in nanocomposites.

Key words: nanocomposites, atomic strain, interfaces, carbon nanotubes.

1. Introduction

Polymer based nanocomposites are a new class of composites that are particle-filled polymers for which at least one dimension of the dispersed particles is in the nanometer range. Three types of nanocomposites can be distinguished depending on dimensions of the dispersed phase are in nanometer scale. When the three dimensions are in the order of nanometers, we are dealing with isodimensional nanoparticles such as spherical silica and aluminum nanoparticles or semiconductor nanoclusters. When two dimensions are in the nanometer scale and the third is larger, forming an elongated structure, we speak about nanotubes and nanowires. Finally, the third type of nanocomposites is characterized by only one dimension in the nanometer range. In this case the filler is present in the form of sheets of a few nanometer thickness and up to one micrometer long. This family of nanocomposites, known as polymer layered crystal nanocomposites, is almost exclusively obtained by the intercalation of the polymer inside the galleries of layered host crystals. Polymer-layered crystal nanocomposites are now commercially available and have been throughout investigated in a large number of publications during last ten years [1–3].

Nanocomposites with elongated structural fillers have recently attracted many investigations. A focus is almost exclusively on nanocomposites with carbon nanotubes (CNT) due to carbon nanotubes unique properties including mechanical, thermal, optical and electrical [4–7]. However, after nearly a decade of research, their potential as reinforcement for polymers has not been fully realized; the mechanical properties of derived composites have fallen short of expectations. Yet, given the magnitude of the carbon nanotubes mechanical properties, strength as high as 200 GPa and elastic moduli close to 1 TPa range, significant improvement on current composites should be possible provided means to harness the nanotubes unique attributes exhibited at nanoscale can be transferred to the macroscale. One of the reasons that these excellent mechanical properties of carbon nanotubes cannot as yet to be utilized to a full extent (not mentioning their high price) is our limited knowledge of physical mechanisms taking place at nanotube-polymer interfaces. The interfacial interaction is an extremely complex process due to continuous evolution of interfacial zones during deformation. The stress transfer between reinforcing nanotube and the polymer matrix critically controls the mechanical properties of nanocomposites under different loading conditions. The experimental evidence of such stress transfer has been reported [8–10]. The random collapse sites of carbon nanotubes are also observed [11]. The load transfer and fragmentation due to axial straining is also present in classical fibre reinforced composite materials [12–13]. However it has to be noticed that interfacial phenomena at nanotube and fibre interfaces are observed and described at different length scales. Nanoscale systems are intrinsically of a discrete nature and the applicability of macroscopic continuum theories at that scale is not always obvious. For instance, the analysis of nanoscale cantilevers using macroscopic beam theory [14] possesses the interpretation problem for cross sectional moment of inertia present in a solution of Euler beam theory. Furthermore, the theory predicts a linear variation of stresses across the cross-section, a situation that is difficult to envisage on the nanoscale. The only cases for which microscopically based derivation of elasticity are documented are uniformly strained lattices. A continuum theory breaks down also for disordered, amorphous systems below a cer-

*e-mail: rp@ime.aau.dk

tain length scale [15–19]. Classical continuum mechanics is size independent which is in contradiction to the physical observations that at the size scale of a few nanometres, deformations and elastic state are size dependent, and a departure from classical mechanics can be expected [20,21].

The atomistic simulations have been developed as an important technique in multiscale modelling attempting to bridge the gap between atomistic/molecular systems and continuum. Large-scale atomistic simulations represent invaluable tool for the study of complex phenomena originating at the atomic scale. However, direct molecular simulation of materials at micro- and meso-scale level seems to be the objective for future atomic memory computers. At present, the largest parallel computing system is able to analyze 70 billion particles which correspond to the material sample in the excess of one micrometer. Continuum models are accessible to analytical techniques that allow for broader investigation of different properties once the fundamental physics from the atomistic model are established. The key point here is that the information involved in these two approaches is biased; i.e., continuum approach is concerned with classical field quantities such as Cauchy stress tensor and small deformation strain tensor whereas these quantities do not have the same format in discrete systems. Merging these approaches can be done either by using more sophisticated continuum models belonging to the family of microcontinuum media and its members [22–24] or elaborating new discrete quantities which are 'dual' and have their appropriate counterpart within the continuum model. The latter is not as simple as it seems due to the ambiguity in stress calculations at atomic level. The concept of Cauchy stress tensor is essentially macroscopic and cannot be used directly to the set of atoms/molecules which constitute a discrete system. The most frequently used form for the stress at atomic level is based upon the Clausius virial theorem, which determines the stress field applied to the surface of a fixed volume containing interacting particles (atoms). It has been shown that the virial stress cannot be directly related to the classical Cauchy stress and several modifications have been proposed [25–28]. It is essential to recognize that the stress at the location of an atom depends on the details of the interatomic interactions and the positions of interacting neighbours. Hence, the atomic stress is a non-local function of the state of the matter at all points in some vicinity of the reference atom, in contrast to the local stress field used in classical continuum theories. It is also not clear how to use the virial stress formula for cases where the interatomic interactions are described by some multibody potential instead of pair potentials, although some attempts have been made [29]. Furthermore, atoms in bonded polymeric chains are subject to bending and torsion moments, which are not included in the definition of virial stress. Nevertheless, the virial stress has become an important calculation tool for evaluating simulations of nanomaterials.

It seems that the relationship between local displacements of atoms and the strain tensor is not ambiguous as the concept of atomic stress. Although different strain measures can be formulated all of them rely on the coordinates of atoms. Given a set of atom coordinates the structure of the molecular system can be analyzed by means of the Voronoi tessellation, which divides space into regions centered on these atoms. A Voronoi cell is the region of space comprising points that are closer to the cell atom than to any other atom. Voronoi cells fill space and define a tessellation. The atomic strain tensor was calculated in [30] to better understand changes in local structure. However, it has not been determined whether or not the sum of local atomic strains corresponds to the total deformation of the simulation cell when loaded by external forces.

In this work we relate a transformation matrix between two deformation states to the strain measure [31] and modify it in order to take into account nonaffine deformations taking place in molecular disordered systems. It is demonstrated that volume average of atomic strains within a simulation cell corresponds to the overall strain imposed on the boundary of the simulation cell. Furthermore, the interfacial sliding between carbon nanotube and surrounding matrix molecules has been predicted as evidenced by experimental results using Raman microspectroscopy technique.

2. Field quantities in discrete systems

2.1. Stress tensor. The most frequently used form for the stress at atomic level is based upon the Clausius virial theorem, which determines the stress field applied to the surface of a fixed volume containing interacting particles (atoms) as follows

$$\sigma_{ij}^{\alpha} = \frac{1}{\Omega^{\alpha}}\left(-m^{\alpha}v_i^{\alpha}v_j^{\alpha} + \frac{1}{2}\sum_{\beta}\frac{\partial V}{\partial r^{\alpha\beta}}\frac{r_i^{\alpha\beta}r_j^{\alpha\beta}}{|\mathbf{r}^{\alpha\beta}|}\right), \qquad \frac{\partial V}{\partial \mathbf{r}^{\alpha}} = \mathbf{F}^{\alpha} = \sum_{\beta\neq\alpha}^{N}\mathbf{F}^{\alpha\beta} \tag{1}$$

where m^{α}, Ω^{α} and v_i^{α} are respectively the atom mass, atomic volume and component of the velocity vector, V is the two-body potential acting between two atoms α and β separated by the distance r, and F^{α} is the total force acting on atom α from all β neighbours. The above expression is well defined only for a system of perfectly equivalent atoms, i.e. a homogeneous system. For systems containing non-equivalent atoms as is the case for either point defects or extended defects alternative prescriptions for defining atomic stress tensor have been suggested in papers [27,32]. The former derives a stress-like formula from a local momentum balance equation using Dirac delta functions and transformation into Fourier space that assumes an atomic system of infinite spatial extent. Furthermore, the second term in Eq. 1 is weighted by the fraction of the length of the α–β bond that is contained within averaging volume

Ω^α, the quantity that is not straightforward to calculate. The latter considers only one-dimensional chain system. Yet another modification of atomic stress was introduced in [28,33]. By using a finite-value and finite-ranged localization function [25] the following expression for the atomic stress can be derived

$$\begin{aligned}\sigma_{ij}(\mathbf{r}) = \sum_\alpha m^\alpha v_i^\alpha v_j^\alpha \psi(\mathbf{r}^\alpha - \mathbf{r}) + \frac{1}{2}\sum_\alpha \sum_{\beta\neq\alpha} \mathbf{r}^{\alpha\beta} \\ \otimes \mathbf{F}^{\alpha\beta} B^{\alpha\beta}(\mathbf{r}) \\ B^{\alpha\beta}(\mathbf{r}) = \int_0^1 \psi(\lambda \mathbf{r}^{\alpha\beta} + \mathbf{r}^\beta - \mathbf{r}) d\lambda, \\ \mathbf{r}^{\alpha\beta} = \mathbf{r}^\alpha - \mathbf{r}^\beta, \quad \psi(r) \approx f\left(\frac{r}{R_c}\right)\end{aligned} \tag{2}$$

where $B^{\alpha\beta}$ is a bond function between atoms α and β representing a weighted fraction of the bond length segment between these atoms that lies within the characteristic volume. The localization function v spreads out the properties of the atoms, and allows each atom to contribute to a continuum property at the position $\mathbf{r}$. This function has units of inverse volume and is non-zero only in some characteristic volume surrounding the spatial point $\mathbf{r}$ and usually is taken as a radial step function f having a constant value within a spherical volume of radius R_c and equals zero outside of the volume. The description of atomic stress contained in Eq. 2 as a function of increasing characteristic volume shows a quicker convergence to values expected from continuum theory than volume averages of the local virial stress [34]. Nevertheless, definitions of atomic-level stress expressed in Eqs. 1 and 2 are known to give unphysical results showing fluctuations of the normal stress components at free surfaces. Attempting to calculate the total stress in the simulation box for systems with stress-nonequivalent atoms it would result in inclusion the contribution of regions where the virial stress is ill defined. Furthermore, a direct calculation of interatomic forces appearing in Eqs. 1 and 2 is not considered as a standard procedure in commercially available molecular dynamics packages, which appears to be a serious obstacle to determine stress state for large molecular systems.

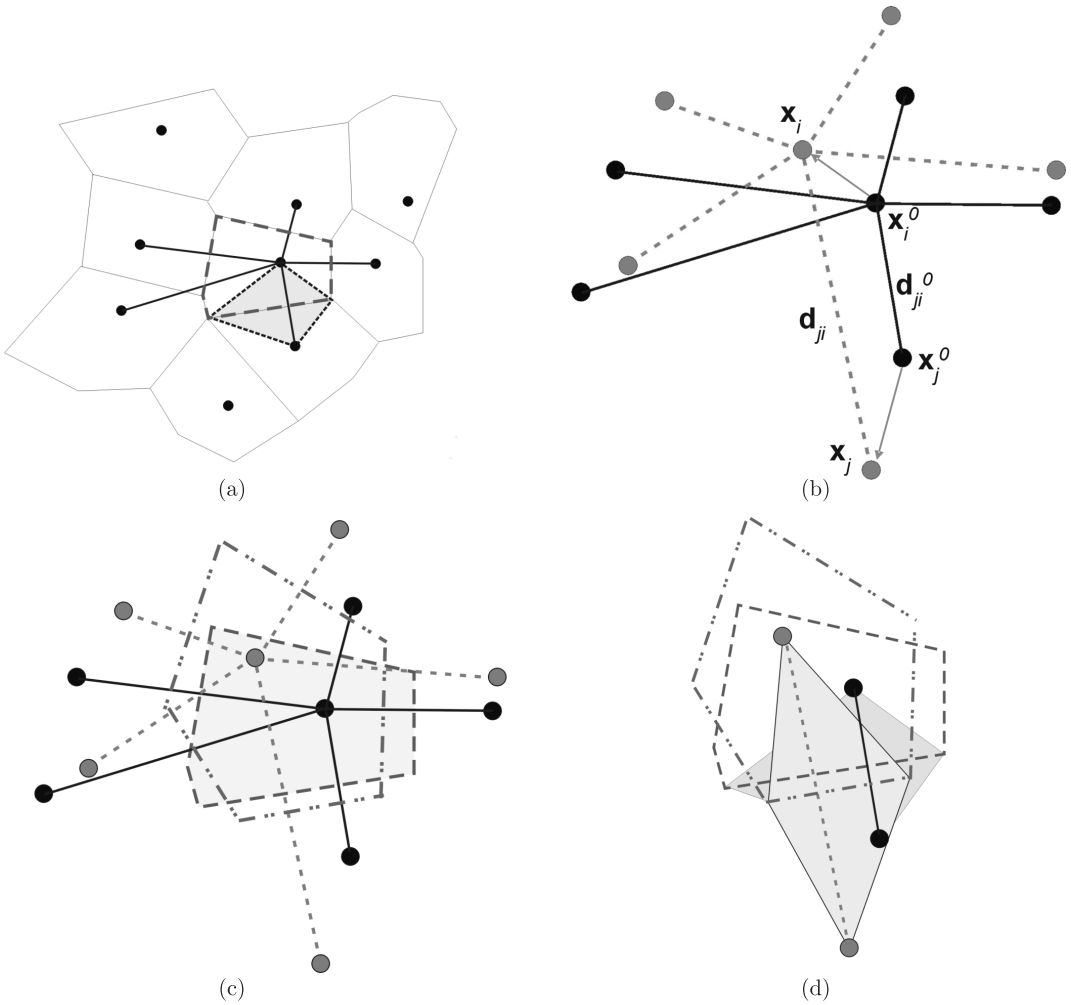

Fig. 1. Tessellation in two-dimensional space: (a) Voronoi polygon and interaction cell between neighbouring atoms, (b) reference and deformed configurations, (c) Voronoi polygon for central atom in reference and deformed configurations, (d) Interaction cells for two neighbouring atoms in reference and deformed configurations

2.2. Strain tensor. It seems that the relationship between local displacements of atoms and the strain tensor is not as ambiguous as the concept of atomic stress. Although different strain measures can be formulated all of them rely on the coordinates of atoms. Given a set of atom coordinates the structure of the molecular system can be analyzed by means of the Voronoi tessellation, which divides space into regions centered on these atoms. A Voronoi cell is the region of space comprising points that are closer to the cell atom than to any other atom. Voronoi cells fill space and define a tessellation [35–37]. Given a set of atom coordinates the structure of the molecular system can be analyzed by means of the Voronoi tessellation, which divides space into regions centred on these atoms. The atoms are assumed to be in their equilibrium positions, and thermal vibrations are averaged. The Voronoi polygon (polyhedron in 3D) around central atom, Fig. 1a is composed of a set of sub-polygons whose number is determined by a number of neighbours to the central atom. Sub-polygons unambiguously determine area (volume in 3D) belonging to the pair of atoms, which can be considered as an interaction cell. During deformation atoms move to new positions, Fig 1b, and the Voronoi polygon associated with the atom changes it shape and size, Fig. 1c. A new interaction cell is created, Fig. 1d, which is described on each subsequent deformation step. Figure 2 shows Voronoi polyhedral construction for two neighbouring atoms sharing a common face and a single interaction cell in three-dimensional case.

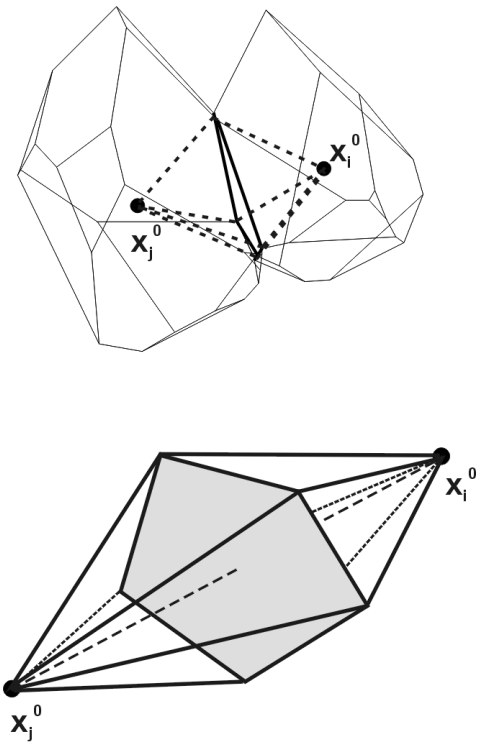

Fig. 2. Tessellation in three-dimensional space

The deformation gradient tensor that provides the best mapping of the present and reference configurations, which include atom and its neighbours, has the following form

$$\mathbf{J}_i = \mathbf{V}_i^{-1}\mathbf{W}_i \tag{3}$$

where

$$\mathbf{V}_i = \sum_{j=1}^{N_i} \mathbf{d}_{ji}^{0T}\mathbf{d}_{ji}^{0} \quad \mathbf{W}_i = \sum_{j=1}^{N_i} \mathbf{d}_{ji}^{0T}\mathbf{d}_{ji}$$

$\mathbf{J}_i$ – represents affine transformation matrix, which minimizes

$$\sum_{j}^{N_i} \left|\mathbf{d}_{ji}^{0}\mathbf{J}_i - \mathbf{d}_{ji}\right|^2$$

whereas $\mathbf{d}_{ji}^{0}$ and $\mathbf{d}_{ji}$ represent distances from central atom (i) to its neighbour (j) in the reference and the present configuration, respectively. The local strain tensor for the atom (i) can be then calculated as

$$\mathbf{E}_i = \frac{1}{2}\left(\mathbf{J}_i\mathbf{J}_i^T - \mathbf{I}\right) \tag{4}$$

The atomic strain tensor is calculated for the central atom and all its neighbours and the total strain is defined as

$$\mathbf{E}^{tot} = \frac{1}{V}\sum_i V_i^p \mathbf{E}_i \tag{5}$$

where V_i^p is the volume of a polyhedron found for the atom (i) and V is the total volume of all polyhedrons within simulation cell.

2.3. Calculation examples. A diamond nanowire loaded in axial tension is shown in Fig. 3 and the tessellation of the reference state is illustrated in Fig. 4. The nanowire has been loaded in three consecutive steps. For each loading step the axial strain calculated from boundary conditions read 0.0250, 0.0514 and 0.0832. Corresponding values obtained from Eq. 5 are 0.0204, 0.0487 and 0.0820. It is clearly seen that the atomic strain obtained from boundary conditions and cell atomic strain gives quite satisfactory results.

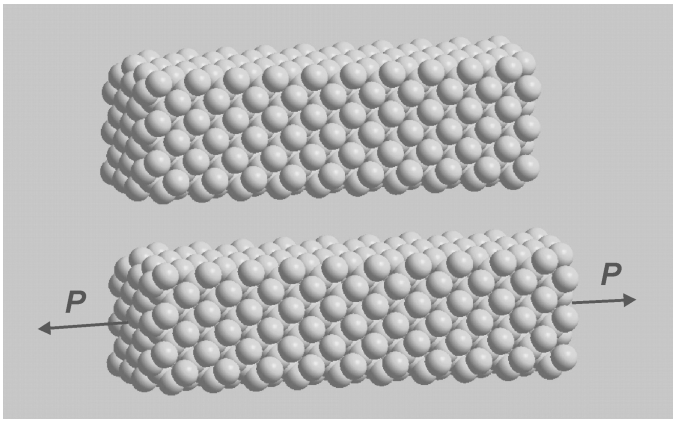

Fig. 3. Diamond nanowire in tension

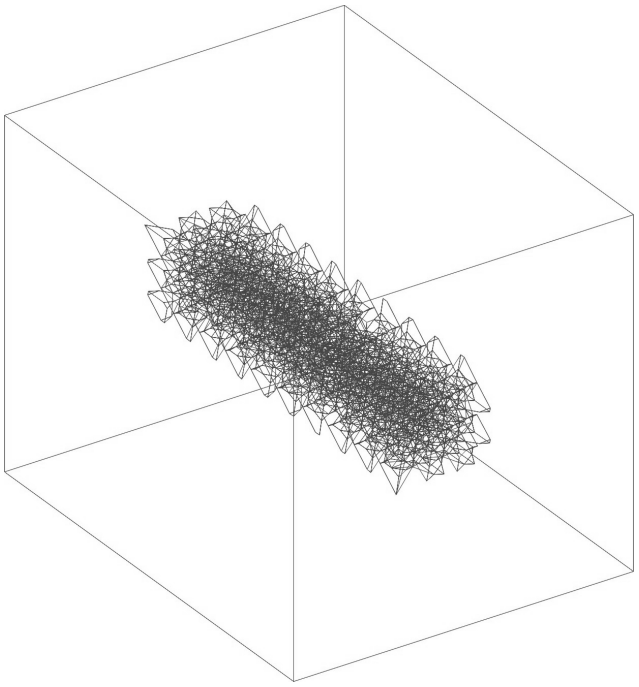

Fig. 4. Tessellation of nanowire in reference configuration

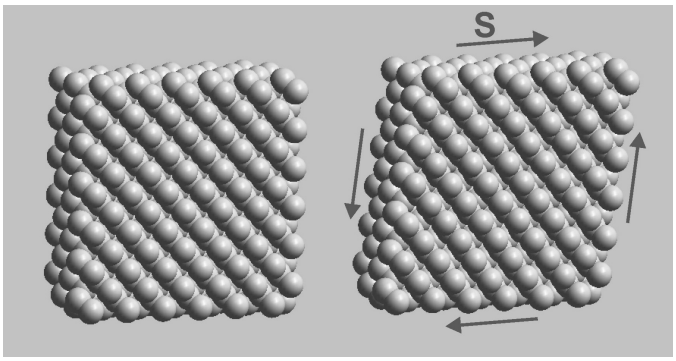

Fig. 5. Quadratic disc in shear

The second example considers shear deformation of a quadratic disc subject to three loading levels. The atomic system and corresponding tessellation for the reference configuration are shown in Figs. 5 and 6. Boundary condition shear strains at consecutive load levels are 0.0248, 0.0656 and 0.2007. Atomic strains are 0.0248, 0.0659 and 0.2138. Also in this example the atomic strain is satisfactory as compared with the boundary condition strain. It should be noted that the third loading step results in large deformation which might be not suitable for the description which assumes small strain conditions. Figure 7 shows disordered molecular system of polypropylene chains. The simulation cell has been subjected to elongation in horizontal direction. Boundary conditions strains are 0.0257 and 0.0482 whereas atomic strains are 0.0209, 0.0414, respectively. In this case atomic strains give significantly underestimated values. The reason for this discrepancy is related to the role of the non-affine displacement field. In disordered systems atomic displacements do not generally become linear to deformation. Each atom moves to its most stable position in response to the deformation of the entire molecular system. These internal displacements are constrained in regular lattice systems resulting in homogeneous deformation. The presence of non-affine deformations invalidates usually accepted Cauchy-Born hypothesis that under the small linear displacement of the simulation cell boundaries all atoms will follow this displacement. However, it appears that under certain conditions even regular crystal structures do not obey this rule [38]. The quantity

$$D_i = \sum_{J}^{N_i} \left| \mathbf{d}_{ij}^0 \mathbf{J}_i - \mathbf{d}_{ij} \right|^2 \tag{6}$$

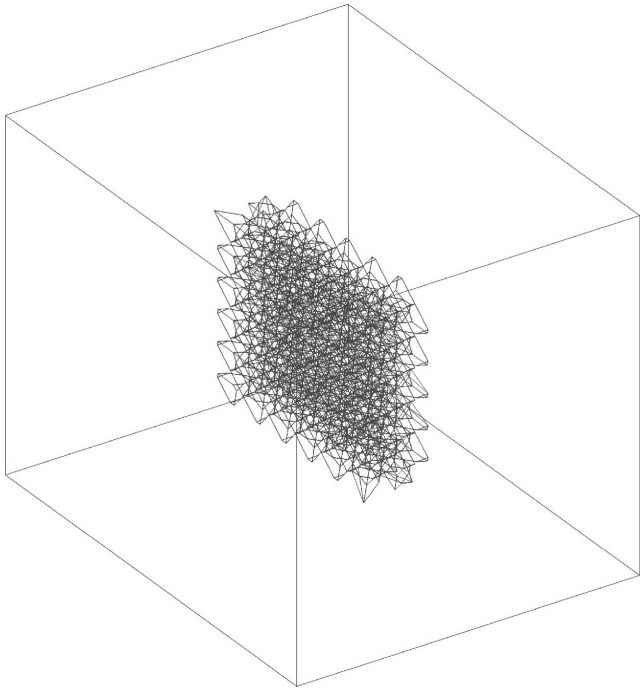

Fig. 6. Tessellation of disc in reference configuration

can be used as the diagnostic for identifying whether the transformation of the reference configuration into present one is close to or far from affine. Small values of D_i indicate affine character of transformation whereas large ones point out the deviation from affine transformation. For the nanowire and disc lattice systems this parameter is very small in the range of 10^{-5} as averaged over all atoms in the system whereas molecular polypropylene system exhibits deviation from affinity hundred times larger. Thus for the systems exhibiting nonaffine deformations the concept of atomic strain has to be modified in order to match overall strains calculated from boundary conditions imposed on the simulation cell.

2.4. Modified atomic strain. The idea is to modify the deformation gradient tensor Ji so as to provide a better match of the reference and present configurations if there is a clear indication that the transformation may deviate from the affine one. Instead of analyzing the central atom and all its neighbours at once the connections

of the atom with subsequent neighbours are treated separately. In other words the Voronoi polyhedra are replaced by a set of interaction cells. For each interaction cell the modified deformation gradient is defined:

$$\mathbf{J}_{ji}^{\mathrm{mod}} = \mathbf{J}_i + \delta\mathbf{J}_{ji} \tag{7}$$

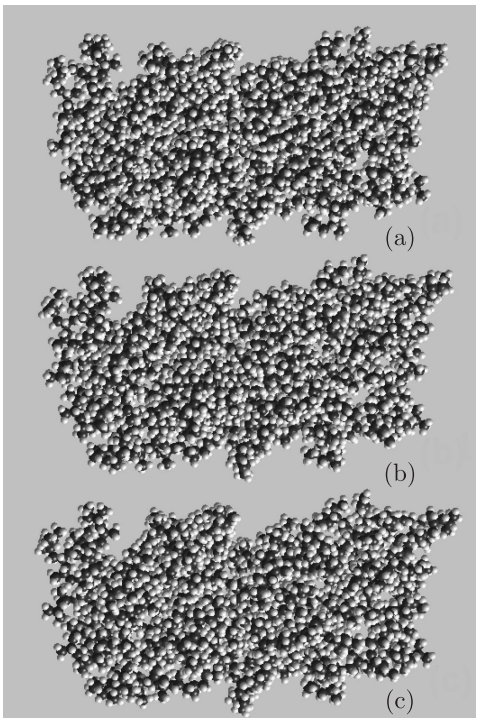

Fig. 7. Polypropylene simulation cell in reference configuration (a) and at two deformation levels (b) and (c)

where J_i stands for the deformation gradient found for the atom (i) according to previously described concept. The corrections δJ_{ji} are determined with the use of an optimization procedure. For each interaction cell the optimization problem is formulated as follows

$$\underset{\text{minimize}}{} \left|\mathbf{d}_{ji}^{0}\mathbf{J}_{ji}^{\mathrm{mod}} - \mathbf{d}_{ji}\right|^2 \tag{8}$$

In order to solve the above problem the Simulated Annealing algorithm has been adopted. For each case the value of maximal allowable correction has been specified. For the lattice systems analyzed above modification of the interaction cell atomic strain does not improve calculations of total strains in any significant way. On the other hand, the modification of polypropylene disordered system with relatively strong non-affinity is significant. The total modified strains have values 0.0256 and 0.0480, which corresponds very well with strains calculated from boundary conditions.

3. Deformation of nanocomposites with carbon nanotubes

3.1. Interfacial sliding. Molecular modeling and molecular dynamics simulations have been performed on all systems presented in this work. Inter- and intramolecular atomic interactions in the polypropylene and polypropylene carbon nanotube composite systems have been modeled using a generic force field DREIDING [45] whereas ab initio COMPASS [46] forcefield has been used for modeling and molecular dynamics simulations of diamond wire and diamond quadratic disk. At first, the system is constructed and subject to energy minimization using Polak-Ribiere conjugate gradient method. Molecular dynamics simulation is performed next, using isothermal-isobaric ensemble (NTP) that keeps temperature and pressure constant, in order to obtain an equilibrium state which simultaneously serves as a reference state. A simple load is applied to the simulation cell in consecutive steps and equilibration is performed after each loading step.

Modified interaction cell atomic strain concept has been applied to analyze a nanocomposite system consisting of polypropylene chains with embedded carbon nanotube, Fig. 8. The nanocomposite has been subject to uniaxial tension along the nanotube axis and the analysis has been performed for eight deformation steps. Figure 9 illustrates stress-strain diagram of the system which is based on calculation of the total strain implementing interaction cell atomic strain modification. It is clearly visible that the departure from linearity occurs at the total strain around 0.01 and one may expect an appearance of non-elastic mechanisms operative in the interior of the molecular system.

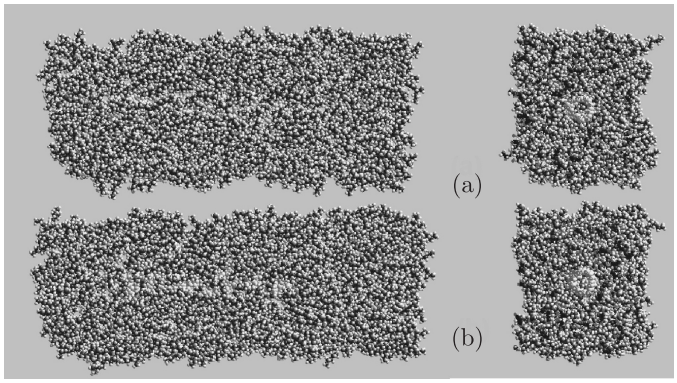

Fig. 8. Carbon nanotube/polypropylene nanocomposite in reference configuration (a) and in deformed state (b)

A number of micromechanical investigations have been performed to predict behaviour of composite interfaces, showing that the detailed behaviour of the material at these interfaces frequently dominates the behaviour of the composite as a whole. In that respect nanocomposite materials are not an exception. On the contrary, since the surface area of nanowires and nanotubes is by a few orders of magnitude larger that corresponding surface area of classical fibres at the same volume fraction, an interpretation of interfacial interaction in nanocomposites becomes a critical issue. This effect is illustrated in Fig. 10, where a conventional fibre and nanotube posses the same aspect ratio equal to 100. Surface area of the fiber is the same as surface area of 36×10^4 nanotubes whereas one needs 22×10^7 nanotubes to fill the volume of the fibre.

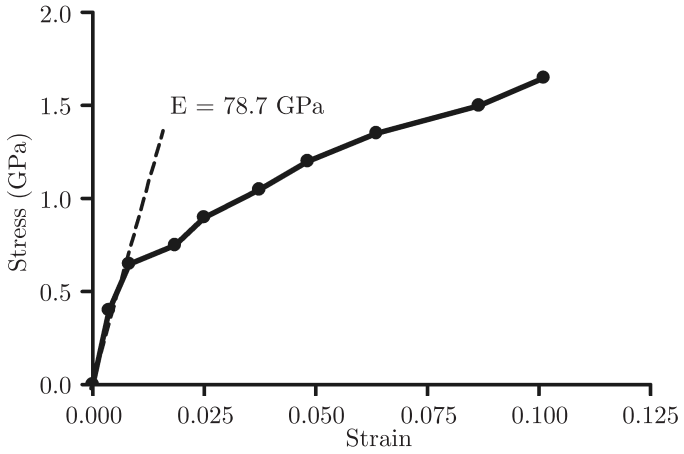

Fig. 9. Stress-strain diagram of the nanocomposite

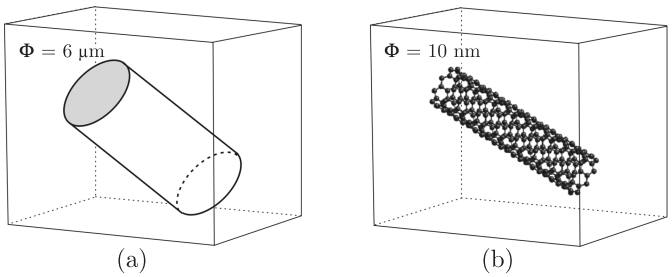

Fig. 10. Geometrical effect of surfaces and volumes

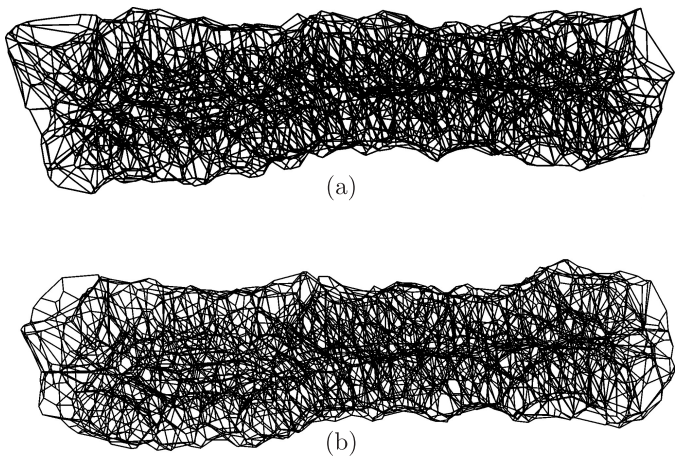

Fig. 11. Voronoi tessellation of carbon nanotube innanocomposite reference (a) and deformed state (b

Thus the geometrical effect of the surface is three orders of magnitude larger than the volume effect. If we assume that the fiber volume fraction in the unit cell in Fig. 10a is 33% then we need only 0.06% volume fraction of nanotubes to get the same surface area of the reinforcement. In this context the concept of interaction cell atomic strain can be very useful allowing to extract surface atoms and investigate a molecular structure in parts or even atom by atom. Figure 11 shows Voronoi tessellation only for atoms belonging to carbon nanotube. These are two configurations being taken from the nanocomposite systems in Fig. 8. An overall strain of the nanotube has been calculated for each deformation level of the nanocomposite using modified interaction cell atomic strain concept, Fig. 12. The nanotube strain follows the strain of nanocomposite to a certain loading level and then lags after it as loading of the nanocomposite increases. This is clear evidence that we need to deal with an interfacial sliding. It should be noticed that initiation of sliding takes place at the same strain level as the departure from the linear behaviour indicated in the stress-strain diagram.

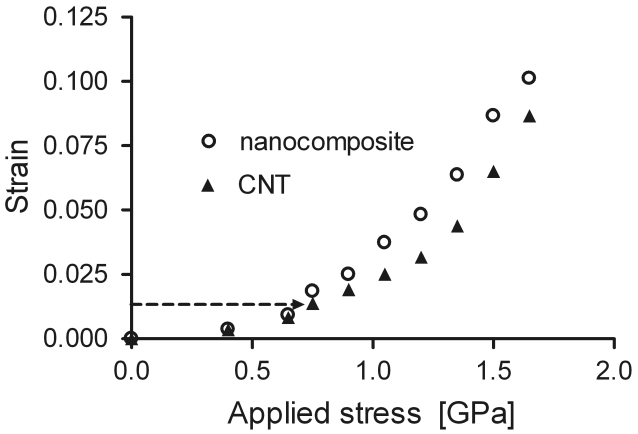

Fig. 12. Evolution of the overall nanotube strain as compared to the total strain of the nanocomposite

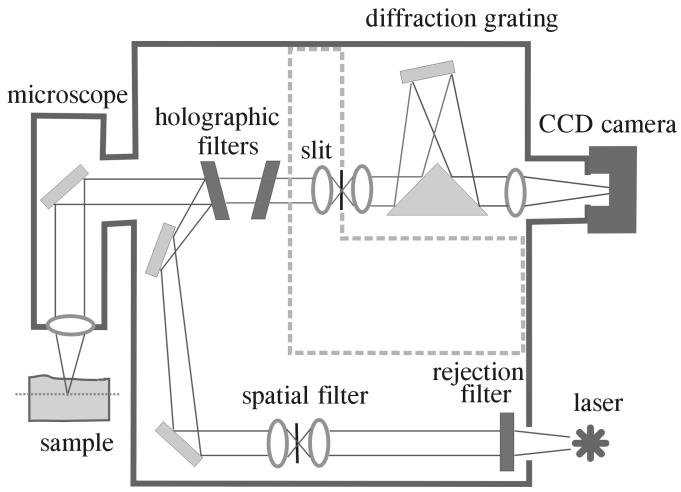

Fig. 13. Schematic chart of the Raman spectra acquisition

3.2. Experimental verification. Single-wall carbon nanotube polypropylene fibres have been manufacture according to the procedure detailed described in [39]. Raman scattering spectra of the nanocomposite fibres were measured in backscattering geometry schematically illustrated in Fig. 13. The fibres were mounted in the mini tensile device for measurements at various strain levels. The Raman spectra of nanotubes have been acquired using the He-Ne 632.8 nm laser. The spot size of the laser

is several orders of magnitude larger than dimensions of the nanotubes and the Raman spectrum is an average response from many nanotubes. The orientation distribution of nanotubes in the polymeric matrix can also be assessed using Raman polarized measurements. The intensity of Raman scattering decreases significantly as the angle between the fibre axis and the polarization direction changes from 0 to 90° which suggests that nanotubes preferential orientation is along fibre axis [39]. The Raman spectrum of nanotubes is shown in Fig. 14.

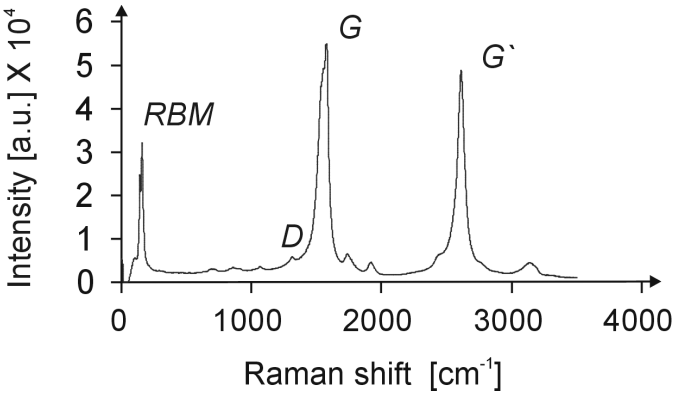

Fig. 14. Raman spectrum of carbon nanotubes

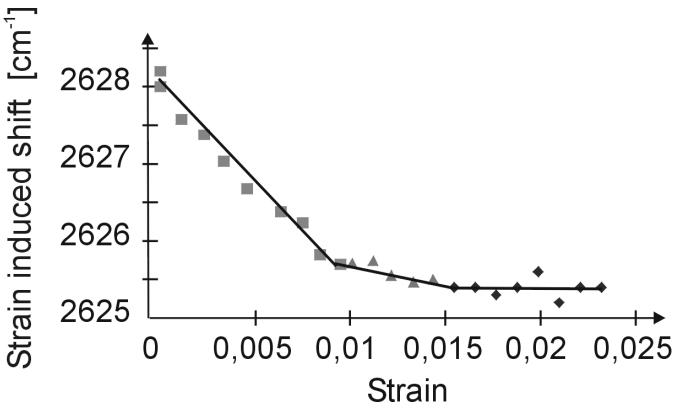

Fig. 15. Strain induced shift of the G‘ Raman peak

The typical Raman spectrum of carbon nanotubes consists of four distinct features. In the low frequency range the radial breathing mode (RBM) is attributed to the simultaneous movement of carbon atoms in the radial direction of the nanotubes. The band is strongly coupled to the diameter of the nanotubes and nanotubes with a particular diameter can dominate RBM spectrum [40]. This coupling can be applied to probe diameters of nanotubes. By applying lasers with different excitation wavelengths RBM frequency will change depending on the nanotube diameter. The D band is related to finite size effects and the presence of disordered elements such as defects in the atomic structure [41]. The frequency of the D band has been shown to be linearly dependent on strain applied to the nanotube [42]. When the nanotube is loaded in tension the frequency moves toward lower wavenumbers while tubes loaded in compression will yield the D band at a higher wavenumbers. The peaks of G band are attributed the tangential stretch modes when the carbon atoms in the nanotubes vibrate in the tangential direction. The last spectral feature appears as G‘ band (also known as D* band) and is strain dependent. The band comes from the second order scattering and is an overtone to the D band. Its intensity is significantly higher than the D band and therefore it is frequently used to detect the deformation of carbon nanotubes. The remaining band observed in Fig. 14 are assigned second order scattering either as overtones or as combination modes.

Figure 15 illustrates strain induced shift in carbon nanotubes embedded in the polypropylene matrix. The strain-peak shift curve changes slope at around 0.01 strain. This value corresponds nicely to the molecular dynamics simulation results and calculations of atomic strains at the interface. The slippage of the nanotubes in the polymer matrix followed by pullout of the tubes from the matrix has been observed in other studies [8,43]. It has been argued [39] that the change of slope is attributed to structural changes in the polypropylene matrix Isotactic polypropylene is mainly composed of α-phase crystalline structure. However during deformation a partial phase change is taking place and β-phase appears which has a lower stiffness and yield stress than the α-phase. This results in a similar change of slope for a pure polypropylene. However it should be bearded in mind that the strain-shift slope beyond 0.01 strain level is not zero indicating that the stress transfer is still taking place. Furthermore, as already stated, the Raman spectrum is averaged over area significantly larger than a single nanotube and this does not preclude that slippage may occur at some of the nanotube interfaces.

4. Conclusions

The atomic strain concept allows analyzing the molecular structure atom by atom, which may give a unique insight into deformation phenomena operative at molecular level such as interface behaviour in nanocomposites. This work demonstrated that the local atomic strain concept is feasible only when it is possible to use it for calculation of overall strain exerted on the simulation cell. Furthermore, presence of non-affine deformations in molecular systems necessitates detailed analysis pertaining to determination of molecular mechanisms responsible for this kind of behaviour. There exists some evidence that at least for cross-linked amorphous systems, the affine transformations are due to molecular stretching whereas non-affine ones are dominated by bending modes [44]. It might be hypothesized that in amorphous molecular systems the deformation of Voronoi polyhedra differs from atom to atom, however there will be no topological changes as long as the deformation is homogeneous and elastic i.e. the number of faces, edges and vertices does not change. In nanostructures subject to inelastic deformation we may expect polyhedral transformation resulting in a change of shape,

size and a change in the number of faces, edges and vertices [37]. Eventually, one could expect to find a relation between topological changes of Voronoi polyhedra and non-affine deformations. In principle, each appropriately selected strain measure is able to provide information on local changes at atomic sites as loading increases. However, the true test of the atomic strain concept is how well it approximates total strain of the simulation cell by summing local atomic strains over all atoms present in the system. In the best case this sum should be equal or very close to the total strain calculated from boundary conditions of the simulation cell as it has been documented in the present work.

An extended simulation study should consider influence of nanowire geometry such as aspect ratio and diameter on interfacial stress distribution, both of which affect stress transfer behaviour. Furthermore, an immobilization of polymer chains in a vicinity of nano-inclusions should be investigated in order to determine an effective domain of reinforcement of the polymeric matrix. All these analyses would be facilitated by the use of atomic strain concept, which allows analyzing the molecular structure atom by atom.

References

[1] P.C. LeBaron, Z. Wang, and T.J. Pinnavaia, "Polymer-layered silicate nanocomposites: an overview", *Applied Clay Science* 15, 11–29 (1999).

[2] M. Alexandre and P. Dubois, "Polymer-layered silicate nanocomposites: preparation, properties and uses of a new class of materials", *Materials Science and Engineering* R 28, 1–63 (2000).

[3] D. Schmidt, D. Shah, and E.P. Giannelis, "New advances in polymer/layered silicate nanocomposites", *Current Opinion in Solid State and Materials Science* 6, 205–212 (2002).

[4] D. Srivastava, C. Wei, and K. Cho, "Nanomechanics of carbon nanotubes and composites", *Applied Mechanics Review* 56(2), 215–230 (2003).

[5] H. Rafii-Tabar, "Computational modelling of thermo-machanical and transport properties of carbon nanotubes", *Physical Reports* 390, 235–452 (2004).

[6] R. Andrews and M.C. Weisenberger, "Carbon nanotube polymer composites", *Current Opinion in Solid State and Materials Science* 8, 31–37 (2004).

[7] E.T. Thostenson, C. Li, and T-W. Chou, "Nanocomposites in context", *Composite Science and Technnology* 65, 491–516 (2005).

[8] L.S. Schadler, S.C. Giannaris, and P.M. Ajayan, "Load transfer in carbon nanotube epoxy composites", *Applied Physics Letters* 73(26), 3842–3844 (1998).

[9] O. Lourie and H.D. Wagner, "Evidence of stress transfer and formation of fracture cluster in carbon nanotube-based composites", *Composite Science and Technology* 59, 975–977 (1999).

[10] J. Gou, B. Minaie, B. Wang, Z. Liang, and C. Zhang, "Computational and experimental study of interfacial bonding of single-walled nanotube reinforced composites", *Computational Materials Science* 31, 225–236 (2004).

[11] H.D. Wagner, O. Lourie, Y. Feldman, and R. Tenne, "Stress-induced fragmentation of multiwall carbon nanotubes in a polymer matrix", *Applied Physics Letters* 72(2), 188–190 (1998).

[12] A.S. Nielsen and R. Pyrz, "Study of the influence of thermal history on the load transfer efficiency and fibre failure in carbon/polypropylene microcomposites using Raman spectroscopy", *Composite Interfaces* 6(5), 467–482 (1999).

[13] E.K. Gamstedt, M. Skrifvars, T.K. Jacobsen, and R. Pyrz, "Synthesis of unsaturated polyesters for improved interfacial strength an carbon fibre composites", *Composites: Part A* 33, 1239–1252 (2002).

[14] E.W. Wong, P.E. Sheehan, and C.M. Lieber, "Nanobeam mechanics: elasticity, strength and toughness of nanorods and nanotubes", *Science* 277, 1971–1975 (1997).

[15] J.P. Wittmer, A. Tanguy, J.-L. Barrat and L. Lewis, "Vibrations of amorphous, nanometric structures: When does continuum theory apply?", *Europhysics Letters* 57(3), 423–429 (2002).

[16] A. Tanguy, J.P. Wittmer, F. Leonforte, and J.-L. Barrat, "Continuum limit of amorphous elastic bodies: A finite-size study of low-frequency harmonic vibrations", *Physical Review B* 66, 174205 (2002).

[17] F. Leonforte, A. Tanguy, J.P. Wittmer, and J.-L. Barrat, "Continuum limit of amorphous elastic bodies II: Linear response to a point source force", *Physical Review B* 70, 014203 (2004).

[18] A. Berezhnyy and L. Berlyand, "Continuum limit for three-dimensional mass-spring networks and discrete Korn's inequality", *J. Mechanics and Physics of Solids* 54, 635–669 (2006).

[19] C. Maloney and A. Lemaître, "Universal breakdown of elasticity at the onset of material failure", *Physical Review Letters* 93(19), 195501 (2004).

[20] H. Liang and M. Upmanyu, "Size-dependent elasticity of nanowires: Nonlinear effects", *Physical Review B* 71, 241403 (2005).

[21] X. Zhang and P. Sharma, "Size dependency of strain in arbitrary shaped anisotropic embedded quantum dots due to nonlocal dispersive effects", *Physical Review B* 72, 195345 (2005).

[22] R. Sunyk, and P. Steinmann,"On higher gradients in continuum-atomistic modelling", *Int. J. Solids and Structures* 40, 6877–6896 (2003).

[23] Y. Chen, J.D. Lee, and A. Eskandarian, "Atomistic viewpoint of the applicability of microcontinuum theories", *Int. J. Solids and Structures* 41, 2085–2097 (2004).

[24] M. Arndt and M. Griebel, "Derivation of higher order gradient continuum models from atomistic models for crystalline solids", *Multiscale Modelling and Simulations* 4(2), 531–562 (2005).

[25] R.J. Hardy, "Formulas for determining local properties in molecular dynamics simulations. Shock waves", *J. Chemical Physics* 76(1), 622–628 (1982).

[26] Z.H. Sun, X.X. Wang, A.K. Soh, and H.A. Wu, "On stress calculations in atomistic simulations", *Modelling and Simulations in Materials Science and Engineering* 14, 423–431 (2006).

[27] J.F. Lutsko, "Stress and elastic constants in anisotropic solids: Molecular dynamics technique", *J. Applied Physics* 64, 1152–1154 (1988).

[28] J. Cormier, J.M. Rickman, and T.J. Delph, "Stress calculation in atomistic simulations of perfect and imperfect solids", *J. Applied Physics* 89(1), 99–104 (2001).

[29] T.J. Delph, "Conservation laws for multibody interatomic potentials", *Modelling and Simulations in Materials Science and Engineering* 13, 585–594 (2005).

[30] P.H. Mott, A.S. Argon and U.W. Suter, "The atomic strain tensor", *J. Computational Physics* 101, 140–150 (1992).

[31] J. Li and F. Shimizu, "Least-square atomic strain", Report, `http://164.107.79.177/Archive/Graphics/A/annotate_atomic_strain/Doc/main.pdf`

[32] K.S. Cheung and S. Yip, "Atomic-level stress in an inhomogeneous system", *J. Applied Physics* 70(10), 5688–5690 ((1991).

[33] M. Zhou, "A new look at the atomic level virial stress: on continuum-molecular system equivalence", *Proc. Royal Society of London A*, 459, 2347–2392 (2003).

[34] J.A. Zimmerman, E.B. Webb III, J.J. Hoyt, R.E. Jones, P.A. Klein, and D.J. Bammann, "Calculation of stress in atomistic simulation", *Modelling and Simulations in Materials Science and Engineering* 12, 319–332 (2004).

[35] R. Pyrz, "The application of morphological methods to composite materials" in: *Comprehensive Composite Materials*, Vol. 2, pp. 553–576, ed. A. Kelly and C. Zweben, Elsevier, Oxford, 2000.

[36] B. Bochenek and R. Pyrz, "Reconstruction of random microstructures - a stochastic optimization problem", *Computational Materials Science* 31, 93–112 (2004).

[37] Z.H. Stachurski and W. Brostow, "Methamorphosis of Voronoi polyhedra as a definite measure of the elastic-to-dissipative atomic displacement transition", *Polymery* 46, 302–306 (2001).

[38] G. Friesecke and F. Theil, "Validity and failure of the Cauchy-Born hypothesis in a two-dimensional mass-spring lattice", *J. Nonlinear Science* 12, 445–478 (2002).

[39] T.E. Chang, L.R. Jensen, A. Kisliuk, R.B. Pipes, R. Pyrz, and A.P. Sokolov, "Microscopic mechanism of reinforcement in single-wall carbon nanotube/polypropylene nanocomposites", *Polymer* 46, 439–444 (2005).

[40] A.M. Rao, E. Richter, S. Bandow, B. Chase, P.C. Eklund, K.A. Williams, S. Fang, K.R. Subbaswamy, M. Menon, A. Thess, R.E. Smalley, G. Dresselhaus, and M.S. Dresselhaus, "Diameter-selective Raman scattering from vibrational modes in carbon nanotubes", *Science* 275, 187–191 (1997).

[41] R. Saito, T. Takeya, T. Kimura, G. Dresselhause, and M.S. Dresselhause, "Finite-size effect on the Raman spectra of carbon nanotubes", *Physical Review B* 59, 2388–2392 (1999).

[42] O. Lourie and H.D. Wagner, "Evaluation of Young's modulus of carbon nanotubes by micro-Raman spectroscopy", *J. Materials Research* 13, 2418–2422 (1998).

[43] P.M. Ajayan, L.S. Schadler, C. Giannaris, and A. Rubio, "Single-walled carbon nanotube-polymer composites: strength and weakness", *Advanced Materials* 12, 750–753 (2000).

[44] D.A. Head, A.J. Levine, and F.C. MacKintosh, , "Deformation of cross-linked semiflexible polymer networks", *Physical Review Letters* 91(10), 108102 (2003).

[45] S.L. Mayo, B.D. Olafson, and W.A. Goddard III, "DREIDING: A generic force field for molecular simulations", *J. Physical Chemistry* 94, 8897–8909 (1990).

[46] `http://www.accelrys.com/mstudio/ms modeling/discover.html`